# Experimental observation of open structures in elemental magnesium at terapascal pressures

# Experimental observation of open structures in elemental magnesium at terapascal pressures

M. G. Gorman,[1,2*] S. Elatresh,[3,8] A. Lazicki,[1] M. M. E. Cormier, [1,4] S. Bonev,[1] D. McGonegle,[5] R. Briggs,[1,2] A. L. Coleman,[1,2] S. D. Rothman,[6] L. Peacock,[6] J. Bernier,[1] F. Coppari,[1] D. G. Braun,[1] J. R. Rygg,[7] D. E. Fratanduono,[1] R. Hoffmann,[3] G. W. Collins,[7] J. S. Wark,[5] R. F. Smith,[1] J. H. Eggert,[1] M. I. McMahon,[2]

[1]*Lawrence Livermore National Laboratory, 7000 East Avenue, Livermore CA 94500, USA*

[2]*SUPA, School of Physics & Astronomy, and Centre for Science at Extreme Conditions, The University of Edinburgh, Edinburgh, EH9 3FD, UK*

[3]*Department of Chemistry and Chemical Biology, Cornell University, Baker Laboratory, Ithaca, New York 14853-1301, USA*

[4]*Department of Physics & Atmospheric Science, Dalhousie University, Halifax, Nova Scotia, CA*

[5]*Department of Physics, Clarendon Laboratory, Parks Road, University of Oxford, Oxford, OX1 3PU, UK*

[6]*Atomic Weapons Establishment, Aldermaston, Reading, RG7 4PR, United Kingdom*

[7]*Department of Physics and Astronomy, University of Rochester, Rochester, New York 14623, USA*

[8]*Physics Department, King Fahd University of Petroleum and Minerals, Dhahran 31261, Saudi Arabia*

**Investigating how solid matter behaves at enormous pressures, such as those found in the**

**deep interiors of giant planets is a great experimental challenge. Over the last decade, computational predictions have revealed that compression to terapascal (TPa) pressures (10 million atmospheres) may bring about counter-intuitive changes to the structure and bonding of solids, as quantum mechanical forces grow in influence [3–8]. Whether this exotic behaviour - known to exist at modest pressures in the highly-compressible light alkali metals [9,10] - is commonplace among high-pressure solids has remained experimentally untested, as studying solids at TPa conditions in the laboratory is incredibly challenging. By compressing a candidate material, elemental magnesium, up to 1.3 terapascals ($\sim$ 4 times the pressure of the Earth's core) using shaped laser pulses and directly probing the crystal structure using nanosecond-duration x-ray diffraction, we found that Mg changes its crystal structure several times with non-close-packed phases emerging at the highest pressures. We demonstrate that phase transformations of extremely condensed matter, previously only accessible through theoretical calculations, can now be experimentally explored.**

At extreme compressions, found in the cores of large rocky exoplanets, it was traditionally believed that solid matter will assemble in close-packed, metallic crystal structures with such stability, that structural rearrangements would be highly unlikely [1,2]. However, the advent of modern computational tools for predicting structure and electronic properties at any arbitrary volume has suggested a new paradigm for a wide range of highly-compressed materials [3–8]. Calculations of matter at TPa pressures indicate that solid materials may adopt non-close-packed lattice arrangements to accommodate clouds of localised valence electrons forced away from the core electrons by Coulombic interactions and Pauli exclusion [11]. Theory predicts that the structure of elemental

Mg will transform multiple times at pressures approaching 1 TPa as the influence of these quantum effects grow. Close-packed structures like hexagonal close-packed (hcp) and face centred cubic (fcc), stable in Mg at ambient and moderate pressures, are predicted to be replaced with hexagonal and cubic structures containing more interstitial space within the lattice [3,4,6,7]. Similar behaviour has been observed in the light alkali metals at more modest pressures due to their high compressibility and low electronegativity [9,10]. It remains unknown if such behaviour is ubiquitous in high-pressure solids, as TPa pressures are inaccessible using standard experimental techniques: TPa pressures are currently incredibly challenging to achieve using static compression methods [12]; and sample heating associated with shock compression precludes the study of solid matter at 1 TPa.

To reach the TPa regime to study solid Mg, we used the National Ignition Facility (NIF) and directly probed the crystal structure at peak pressure with nanosecond-duration x-ray diffraction. Our experiments reveal four new, distinct, non-close-packed structures of Mg at 0.31 TPa, 0.56 TPa, 0.96 TPa and 1.32 TPa. Diffraction at the highest pressures is consistent with the formation of simple hexagonal (sh) and simple cubic (sc) phases in agreement with decade old computational predictions [6,7]. These results represent the highest-pressure solid-solid phase transformations observed, and offer the first experimental insights into how pressure-induced quantum effects can drive structural stability at extreme conditions.

We used 16 beams of the NIF to launch an ablatively-driven uniaxial-compression wave into a Mg sample (see Methods). The ramp-shaped laser pulse allows the sample to achieve a

high compression at cool enough temperature to remain in the solid state. Pressure in the sample gradually increases over the 25 ns duration of the laser pulse, before pressure uniformity is achieved for several nanoseconds at peak compression. The target package consisted of a 50 $\mu$m thick polycrystalline Mg foil sandwiched between a Be anvil, coated with a thin Au preheat shield, and a diamond window (See Supplementary Fig. 1 and Table S1). This target assembly was placed at the front of the TARget Diffraction In Situ (TARDIS) diagnostic (Fig. 1) [13]. A Ge backlighter foil, positioned near the front surface of the TARDIS, was irradiated by 24 beams of the NIF for 2 ns to produce quasi-monochromatic He-$\alpha$ radiation (characteristic x-ray wavelength of 1.209 Å) [14]. The x-ray pulse was timed to probe the sample once it had achieved a uniform pressure state. Diffraction was collected in a transmission geometry on x-ray sensitive image plates placed on the inside top, bottom and rear surfaces of the TARDIS box. Figure 1 shows a representative diffraction pattern in stereographic projection such that the Debye-Scherrer diffraction rings appear as concentric circles. The rear surface velocity of the diamond tamper was measured in each experiment using the VISAR (Velocity Interferometry System for Any Reflector) diagnostic [15] which, using the known equation of state of diamond [16,17], determines the sample pressure history [13]. Sample temperatures were not measured in these experiments but are estimated to range from 2500 K at 0.31 TPa to 5000 K at 1.32 TPa from radiation-coupled hydrodynamic simulations (Supplementary Information).

We observed four distinct phases of Mg up to 1.32 TPa. Figure 2a displays four representative diffraction images collected at 0.31 TPa, 0.56 TPa, 0.96 TPa and 1.32 TPa, projected such that the Debye-Scherrer diffraction rings appear as vertical lines of constant scattering angle. The

azimuthally-averaged 1D profiles for all experiments are shown in Figure 2b with the diffraction peaks from compressed Mg shaded. In some experiments, non-sample diffraction peaks were observed either from the Be pusher, Au heat shield or single crystal diamond window (Supplementary Figs. 2-7). Six diffraction reflections from the compressed Mg sample were visible at 0.31 TPa (Fig. 2b). By analysing the location of these reflections, it is clear that the bcc phase which is predicted to be stable at these conditions, cannot explain all observed reflections. However, the diffraction data are consistent with a bcc-like structure given the location of the strongest reflections are similar to those predicted for bcc, in addition to the observation of weaker diffraction peaks (Fig. 3a). While we propose a structural candidate, a bc6 structure, which explains all reflections and gives a reasonable density, (Supplementary Fig. 8) it was calculated to have significantly higher enthalpy than the bcc phase. We are therefore unable to unambiguously determine the structure of this phase. A similar diffraction pattern, suggestive of a similar structure was also collected at 0.41 TPa (Fig. 2b and Supplementary Fig. 7).

At 0.56 TPa, five diffraction reflections from the Mg sample were observed (Fig. 2b). The fcc phase which is predicted to be stable at these conditions could not explain all observed reflections [7]. However, as before, diffraction peaks in similar locations to those predicted from fcc, as well as the observation of several weak reflections, pointed towards the actual structure being a distortion of fcc. Indeed, it was found that a structure with space group symmetry F$mmm$ (Z = 4) explained all observed reflections (Fig. 3a) and was energetically competitive with fcc (Supplementary Fig. S13). This new phase of Mg is an orthorhombic distortion of fcc with the main structural changes involving an $\sim$11 % contraction of the *a* lattice parameter and a $\sim$15 % expansion of the *c* lattice

parameter with little relative change to the *b* axis. The measured lattice parameters are *a* = 2.58(1) Å, *b* = 2.91(1) Å and *c* = 3.35(1) Å.

At 0.96 TPa, two diffraction peaks from the Mg sample were observed. While we are unable to unambiguously determine the structure from this data, the diffraction is consistent with the simple hexagonal structure (space group symmetry P6/mmm (Z=1)), predicted to be the stable structure at these conditions [7]. Assuming the sh structure, the measured $c/a$ ratio (c/a=0.87(1)) agrees well with the prediction from previous DFT calculations (c/a=0.90) [4,7] adding confidence to our assignment of this phase. The measured lattice parameters are *a* = 1.87(1) Å and *c* = 1.63(1) Å. Furthermore, the d-spacings of the two observed reflections were compared with density functional theory (DFT) predictions for energetically-favorable high pressure phases (Fig. 3a and Supplementary Fig. S9) and shown to only be consistent with the sh phase, within experimental uncertainty. Given the low signal to noise of the diffraction data at 0.96 TPa, there may be other weak diffraction lines present which we are unable to resolve. However, as we see no evidence of other diffraction lines, we choose to make the simplest interpretation of the data that is also supported by theoretical predictions [7]. One diffraction peak observed at 0.41 TPa, 0.56 TPa and 0.96 TPa is consistent with a bcc phase of Be, the material used as the pusher in these experiments (Fig. 3a, Supplementary Figs. 11-12 and table S2). This is the first experimental observation of this phase, which has been predicted to become stable above 0.3 TPa [18–21].

At 1.32 TPa, the observed diffraction pattern also showed two peaks. Again, while we are unable to definitively determine the structure of the Mg sample at these conditions, the two diffrac-

tion peals are consistent with the simple cubic structure (space group symmetry Pm3m (Z=1)) predicted to be stable at these conditions [7]. Observed d-spacings were again compared to DFT predictions for the candidate phases at 1.32 TPa (Fig. 3a and Fig. S10), and only the simple cubic phase assignment is consistent, within experimental uncertainty. As with the diffraction collected at 0.96 TPa, we cannot rule out the presence of additional weak diffraction peaks in the data but choose the simplest interpretation of the data which is that the sample forms the sc structure, in agreement with theoretical predictions [7]. The sc lattice parameter is $a$ = 1.60(1) Å . This is the highest-pressure structural phase transformation observed, the first above 1 TPa and corresponds to ∼5.5-fold compression of Mg

The measured pressures and densities of the assigned Fmmm, sh and sc phases are compared to density functional theory (DFT) predictions in Fig 3b. The density for the phases observed at 0.31 TPa and 0.41 TPa was calculated assuming a bcc phase, using the reflections consistent with bcc, since a likely phase assignment was not found for the apparently distorted structure (see Supplementary table S3 for more information on measured diffraction locations, densities and uncertainties). We investigated this unexpected observation of non-close-packed structures at 0.31 TPa, 0.41 TPa and 0.56 TPa (fcc was predicted to be stable to 0.76 TPa [7]) by performing structure searches at 0 K. We found several lower-symmetry phases (Supplementary Fig. 13) which are energetically competitive at these conditions. Among them is the othorhomic Fmmm phase observed experimentally, which lies within 20 meV of the stable fcc phase. This suggests that elevated temperatures present in the ramp-compressed Mg (∼4200 K predicted, see Supplementary Information) may stabilize the Fmmm phase, a surprising result as symmetry-breaking transitions

are commonly considered to be low temperature phenomena [22]. However, phonon free energy calculations within the quasi-harmonic approximation show that the F$mmm$ phase of Mg has larger entropy (S) than fcc such that at elevated temperatures, the Gibbs free energy (G = H - TS) of F$mmm$ becomes lower than fcc (Supplementary Fig. 13). The F$mmm$ phase was also found to be dynamically stable with no negative phonon frequencies (Supplementary Fig. 14).

The key finding of this study is the experimental observation that non-close-packed structures do become stable at terapascal pressures and over 5-fold compression, confirming what theoretical calculations for Mg and other elemental systems have been predicting over the last decade [3,4,6,7]. The drop in coordination number from 12 in ambient hcp Mg to 8 in the sh phase at 0.96 TPa and 6 in the sc phase at 1.32 TPa contradicts our traditional understanding that crystals should pack more efficiently with increasing compression [1,2]. However, similar predictions at terapascal pressures for several other elemental systems such as C [5], Al [6] and Si [8] suggest that this behavior could be quite general. At extreme compression, as valence electron density is forced away from atomic sites due to Coulomb effects and Pauli exclusion, the system can be stabilized by forming electride structures, in which charge is localized into interstitial sites in the lattice. Structures such as sh and sc, which are energetically unfavourable configurations at ambient conditions due to their low atomic packing fractions (sh - 60 % , sc - 52 %), emerge as the most stable configurations at terapascal pressures as their larger interstitial regions mean they can accommodate localized charge density more easily than close-packed structures (74 % atomic packing fraction) (Supplementary Fig. 13). In figure 4, we show calculations of the electronic localisation function (ELF) for the observed and predicted structures of Mg (yellow regions in each unit cell) (see Methods). Our calculations,

as well as previous studies [6,7], have predicted that valence charge accumulates in the interstitial regions of sh-Mg, centred at the 2d ($\frac{1}{3}$, $\frac{2}{3}$, $\frac{1}{2}$) Wyckoff site of the sh lattice (Fig. 4) and the 1b ($\frac{1}{2}$, $\frac{1}{2}$ ,$\frac{1}{2}$) Wyckoff site of the sc lattice (Fig. 4) forming pseudo-ionic $MgE_2$ and MgE structures (E denotes localised-electron pseudo-anions), analogous to the $AlB_2$ and CsCl structures. We suggest that the direct observation of the sh and sc phases of Mg is the first experimental evidence of how core-valence and core-core electron interactions can influence material structure at terapascal pressures. Figure 4 shows our revised temperature-pressure phase diagram of Mg to 7000 K and 1.4 TPa. Our experiments compliment previous 0 K theoretical investigations and have mapped out high temperature regions of the Mg phase space, discovering new distorted cubic structures between 0.31 TPa - 0.56 TPa as well as the simple hexagonal and simple cubic structures at 0.96 TPa and 1.32 TPa.

Using x-ray diffraction, we report four new phases of Mg up to 1.32 TPa giving the first experimental insight into phase transformations in extremely compressed solids above 1 terapascal. Our diffraction measurements show clear evidence of non-close-packed, open structures emerging as the most stable configurations at terapascal pressures, providing experimental evidence for the formation of novel electride states and confirming decade-old predictions.

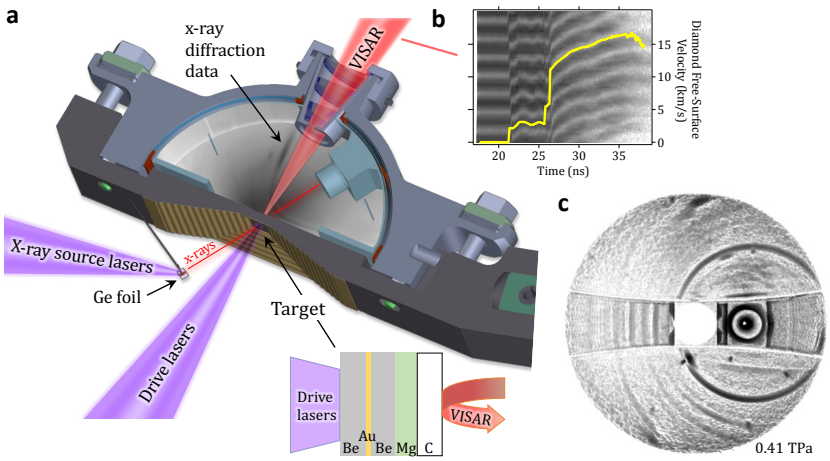


Figure 1: Experimental setup of the TPa NIF diffraction experiments. a) The Mg sample is situated at the front of the TARDIS box where it is compressed by a temporally shaped laser pulse. A typical target assembly is shown. Laser irradiation of a Ge foil generates a $\sim$10.2 keV x-ray source which probes the sample at peak compression. The diffraction pattern is collected on x-ray sensitive image plates situated within the TARDIS diagnostic. b) Representative free surface velocity history as measured by VISAR in each experiment c) A stereographic projection of a representative diffraction data collected at 0.41 TPa.

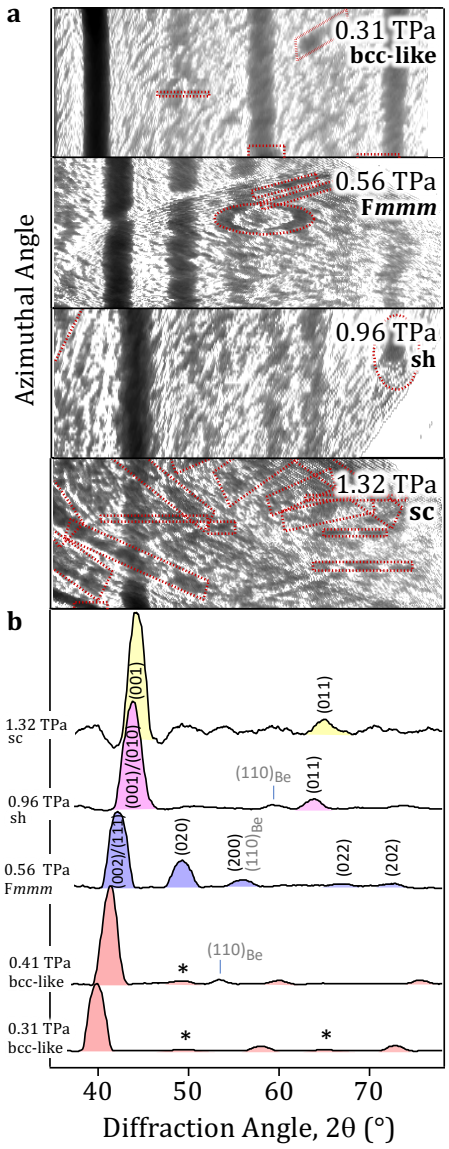


Figure 2: a) Four representative 2D diffraction images which were collected at 0.31 TPa, 0.56 TPa, 0.96 TPa and 1.32 TPa and projected into $\phi$ - $2\theta$ space. b) Corresponding azimuthally-averaged diffraction data. Diffraction from the Mg sample is highlighted by shading and the miller indices of the determined phases are labelled where possible. Non-sample, or non diffraction features in the 2D image have been masked out for clarity (red-dashed enclosures). Weak reflections, inconsistent with the bcc phase are highlighted in the 0.31 TPa and 0.41 TPa profiles with black asterisks.

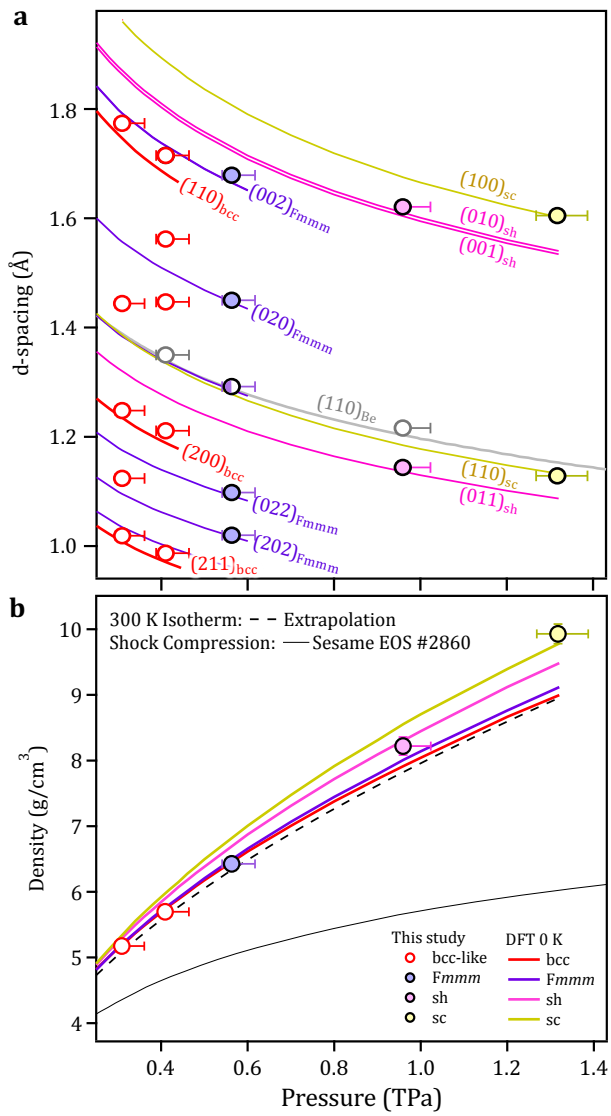


Figure 3: (a) Comparison of measured d-spacings (circles) with DFT simulations for the bcc, Fmmm, sh and sc phases of Mg and the bcc phase of Be (coloured lines). The simulated bcc lines are shown to highlight the similarities with some of the measured d-spacings at 0.31 TPa and 0.41 TPa. (b) Calculated pressure-density relations for various phases of Mg with experimentally-determined values overlaid. An extrapolation of the PV relation of bcc Mg from 300 K static compression [28], and the PV relation for shock compressed Mg from SESAME EoS 2860 [29,30] is also shown for comparison.

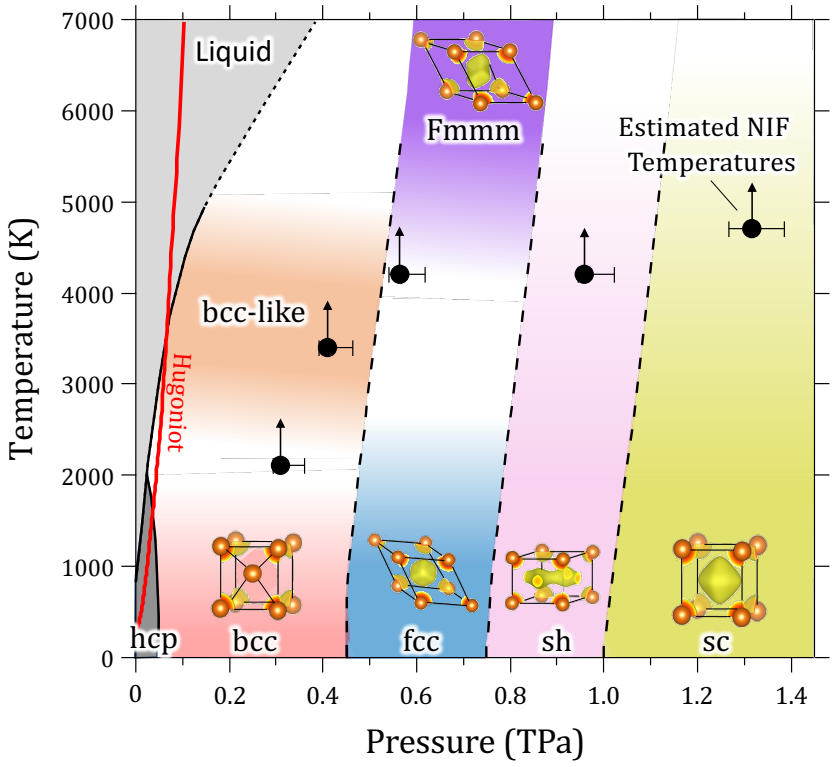


Figure 4: Pressure-temperature phase diagram of Mg constructed using static compression (black lines) [28] and previous DFT calculations (dashed lines) [7]. The black circles represent estimates of Mg temperatures for the NIF experiments based on hydrocode simulations which incorporate radiation coupling and thermal transport models (See Supplementary Information). The conventional unit cells of the stable phases as well as the localised valence charge are displayed (yellow regions). High temperature regions representing the bcc-like and F$mmm$ regions are indicated.

## Methods

### Experimental Methods

Experiments were performed at the National Ignition Facility at the Lawrence Livermore National Laboratory. Targets consisted of a 50 $\mu$m polycrystalline Mg foil, sandwiched between a 200 $\mu$m diamond window and a 20 $\mu$m Be pusher which was bonded to a 40 $\mu$m Be ablator (Fig. 1). We use a double-sided non-contact ZYGO white-light interferometer to measure a 3-D surface optical profile (x-y spatial dimension and z height relative to a reference measurement) of all parts before assembly and again during assembly after each subsequent epoxy layer is added, resulting in a thickness uncertainty of less than 0.2 $\mu$m for each component. More details can be found in [13]. Thin coatings of Re and Au were deposited between the pusher and ablator to protect the sample from x-ray heating from the drive plasma and the x-ray source. The target package was mounted onto a 400 $\mu$m diameter pinhole made of U + 6%Nb, which was positioned on the front of the TARget Diffraction In Situ (TARDIS) diagnostic (Fig. 1) [13]. After background subtraction [13] the 2D diffraction images were azimuthally-averaged to give 1D diffraction profiles. To perform the calibration of the system geometry diffraction lines from a compressed sample are used as input features for an optimization routine as described in Rygg et al ([13]). Each diffraction line is constrained to have the same $2\theta$ along a given Debye Scherer arc which assumes effects of pressure non-uniformity, sample strength, or finite grain size do cause two theta distortions to the diffraction lines. Samples were compressed using 16 beams of NIF with temporally shaped laser pulses of 25 ns in duration and peak intensity up to $1 \times 10^{14}$ W/cm$^2$. The drive beams are incident 40-46$^\circ$ from normal and 1 mm continuous phase plates are used to smooth the beam profile. The

drive beams are pointed into four quadrants to achieve a $\sim$1.8 mm drive spot. This configuration has demonstrated to achieve transverse uniformity in the drive sample [13]. A typical pulse shape used in these experiments is shown in Fig. S17. Quasi monochromatic x-rays where generated by irradiating a Ge foil with 24 beams of NIF with a 2 ns laser pulse of peak intensity $2 \times 10^{15}$ W/cm$^2$. The x-rays are emitted isotropically from the Ge foil. Diffracted x-rays from the Mg sample are collimated by the pinhole and collected on a set of x-ray sensitive image plates in the TARDIS diagnostic. Plastic and Ge filters are placed in front of the image plates to absorb unwanted x-rays. While we use the term pressure throughout the manuscript, our samples are uniaxial compressed. The presence of deviatoric stress states (not measured) due to high pressure strength would potentially result in states which deviate from ideal hydrostaticity.

**Theoretical Methods**

First-principles structure searches, enthalpy calculations, and molecular dynamics simulations (FPMD) were performed with the Vienna *ab initio* simulation package (VASP) [32] within the Perdew-Burke-Ernzerhof generalized gradient approximation (PBE-GGA) [33] of DFT. We used a ten electron projector augmented wave (PAW) pseudopotential (PP) from the VASP library with 800 eV plane wave cut off and 1.7 Bohr outmost core radius. Initially we performed FPMD simulations of liquid Mg along the 10000 K isotherm over the pressure range of interest. These were carried out with 128 atom supercells in the canonical (constant volume, temperature, and particle number) ensemble, with the ($\frac{1}{4}$, $\frac{1}{4}$ ,$\frac{1}{4}$) k-point sampling of the Brillouin zone (BZ), Fermi-Dirac smearing, and a Nosse-Hoover thermostat with a 1 fs ionic time step. The liquid was quenched at

pressures around 350 and 650 GPa until signs of solidification appeared. From the lowest temperature liquid ($T$ ∼5000 K) obtained at each pressure random configurations were taken with cluster sizes between 2 and 10 Å, for which full structural optimisation was carried out. The optimizations were carried out at (target) pressures of 0.32, 0.6, and 0.96 TPa. Overall, about 300, 400 and 100 configurations were generated and optimised at each of the three pressures, respectively, with the number of atoms ranging from 1 to 30. To confirm that this search procedure is exhaustive, we carried out additional genetic structure search and adaptive metadynamics calculations using the Universal Structure Predictor Evolutionary Xtallography (USPEX) package [23–27]. These were carried out with 20-30 hereditary generations, starting with 60 random structures with unit cells of 1 to 28 atoms, 50% of each generation used to create the next, and k-point sampling with a reciprocal space resolution of 0.039. However, no additional competitive structures were found. The enthalpies of the most competitive structures within a 50 meV/atom window found by the liquid sampling method method at 0.32, 0.6, and 0.96 TPa were then computed in the range from 0 to 1.3 TPa. For the final structural calculations and enthalpy computations the BZ was sampled with dense k-point meshes, sufficient to ensure enthalpy convergence better than 1 meV/atom (22 ×22 ×22 for fcc and sc, 28 ×28 ×28 for bcc and sh, 18x18x18 for hcp, 24 ×24 ×24 for F$mmm$ (Supplementary table S4), 36 ×36 ×36 for Immm and R-3m, and 6 ×6 ×6 for Pnma. The accuracy of the VASP PP to describe Mg at the highest pressure considered here was verified by carrying out additional calculations with the Abinit code [34] and using a norm-conserving PP with 1.56 Bohr outmost core radius and 1360 eV cut off. Finally, phonon and Gibbs free energy calculations were performed within the DFT perturbation theory [35] as implemented in Abinit. The

dynamical matrices were computed on uniform 5 $\times$5 $\times$5 **q**-point meshes in the BZ, from which interatomic force constants were obtained and used to interpolate the phonon dispersions on 38 $\times$38 $\times$38 **q**-point meshes. As discussed in the main text, we find from first-principles theory that Fmmm trends towards stability over fcc-Mg at very high temperature. However, we note that the energy differences between fcc and Fmmm are rather small and anharmonic effects are neglected in the quasi-harmonic Gibbs free energy calculations and therefore this method cannot be used to accurately predict the transition temperature, but rather indicate the trend with increasing temperature. In order to quantify the degree of interstitial electron localisation (yellow regions of unit cell in Fig. 4), we computed the electron localisation function (ELF) from 0 K unit cells at selected pressures. ELF $= 0.5$ corresponds to the electron gas (i.e. delocalised electrons) and ELF $= 1.0$ corresponds to perfect localisation. We deemed ELF $> 0.75$ to correspond to localised electrons. We then partitioned the charge density in regions where ELF $> 0.75$ and ELF $< 0.75$. Integrating the interstitial region where ELF $> 0.75$ gave the number of localised electrons. It is worth noting that absolute magnitudes depend on the choice of ELF cutoff but the general trend is not so sensitive to this choice.


1. C. T. Prewitt, R. T. Downs, *Reviews in mineralogy* **37**, 283 (1998).

2. W. Grochala, R. Hoffmann, J. Feng, N. W. Ashcroft, *Angewandte Chemie International Edition* **46**, 3620 (2007).

3. M. S. Miao, R. Hoffmann, *Acc. Chem. Res.* **47**, 1311 (2014).

4. M. S. Miao, R. Hoffmann, *Acc. Chem. Res.* **137**, 3631 (2015).

5. M. Martinez-Canales, C. J. Pickard, R. J. Needs, *Physical Review Letters* **108**, 45704 (2012).

6. C. J. Pickard, R. J. Needs, *Nature Materials* **9**, 624 (2010).

7. P. Li, G. Gao, Y. Wang, Y. Ma, *The Journal of Physical Chemistry C* **114**, 21745 (2010).

8. R. Paul, S. X. Hu, V. V. Karasiev, *Physical Review Letters* **122**, 125701 (2019).

9. Y. Ma, *et al.*, *Nature* **458**, 182 (2009).

10. M. Hanfland, N. E. Christensen, D. L. Novikov, *Nature* **408**, 174 (2000).

11. B. Rousseau, N. W. Ashcroft, *Phys. Rev. Lett.* **101**, 046407 (2008).

12. N. Dubrovinskaia, *Science Advances* **2**, 7 (2016).

13. J. R. Rygg, *et al.*, *Review of Scientific Instruments* **91**, 043902 (2020).

14. F. Coppari, *et al.*, *Review of Scientific Instruments* **90**, 125113 (2019).

15. P. M. Celliers, *et al.*, *Review of Scientific Instruments* **75**, 4916 (2004).

16. D. K. Bradley, *et al.*, *Physical Review Letters* **102**, 75503 (2009).

17. R. F. Smith, *et al.*, *Nature* **511**, 330 (2014).

18. L. X. Benedict, *et al.*, *Phys. Rev. B* **79**, 064106 (2009).

19. R. G. Legrand, *et al.*, *Phys. Rev. B* **82**, 10 (2010).

20. F. Luo, *et al.*, *J. App. Phys. A* **11**, 5 (2012).

21. C. J. Wu, *et al.*, *J. Phys. Chem. A* **125**, 7 (2021).

22. S. Chandrasekhar, *Liquid Crystals*, Cambridge University Press (1992).

23. A. R. Oganov, C. W. Glass, *The Journal of Chemical Physics* **124**, 244704 (2006).

24. A. R. Oganov, A. O. Lyakhov, M. Valle, *Acc. Chem. Res.* **44**, 227 (2011).

25. A. O. Lyakhov, A. R. Oganov, H. T. Stokes, Q. Zhu, *Computer Physics Communications* **184**, 1172 (2013).

26. Q. Zhu, A. R. Oganov, A. O. Lyakhov, X. Yu, *Phys. Rev. B* **92**, 024106 (2015).

27. Q. Zhu, A. R. Oganov, A. O. Lyakhov, *CrystEngComm* **14**, 3596 (2012).

28. G. W. Stinton, *et al.*, *Physical Review B* **90**, B03208 (2014).

29. J. D. Johnson, S. P. Lyon, Technical Report No. LA-UR-92-3407 (unpublished), *Tech. rep.*, Los Alamos National Laboratory (1992).

30. S. P. Marsh, *LASL shock Hugoniot data*, vol. 5 (Univ of California Press, 1980).

31. S. D. Rothman, *et al.*, *Journal of Physics D: Applied Physics* **38**, 733 (2005).

32. G. Kresse, J. Hafner, *Physical Review B* **47**, 558 (1993).

33. J. P. Perdew, K. Burke, M. Ernzerhof, *Phys. Rev. Lett.* **78**, 1396 (1997).

34. X. Gonze, *et al.*, *Computer Physics Communications* **180**, 2582 (2009).

35. X. Gonze, *Phys. Rev. B* **55**, 10337 (1997).

36. G. Zimmerman, *et al. J. Opt. Soc. Am* **68**, 549 (1978).

37. Y. T. Lee, *et al. Phys. Fluids* **27**, 1273 (1984).

**Acknowledgments** We thank the National Ignition Facility staff and the National Ignition Facility Discovery Science programme. This work was performed under the auspices of the US Department of Energy by Lawrence Livermore National Laboratory under contract number DE-AC52-07NA27344. J.S.W. thanks the UK EPSRC for support under grants EP/J017256/1 and EP/S025065/1. M.I.M. thanks the UK EPSRC for support under grants EP/J017051/1 and EP/R02927X/1. M.I.M. is grateful to AWE for the award of a William Penney Fellowship. D.McG. was supported by LLNS under contract number B595954. Partial funding for G.W.C. and J.R.R. was provided by NSF Physics Frontier Center award PHY-2020249 and DOE NNSA award DE-NA0003856.

**Author Contributions** M.I.M. and J.H.E. conceived the work. M.G.G., A.L., D.McG., J.R.R., R.F.S., A.L.C., R.B. performed the experiments. S.E., S.B., and M.M.E.C, performed the first principles calculations. D.G.B., S.R and L.P designed the laser pulse shapes. A.L., J.H.E, and M.G.G analysed the data with assistance from J.B., J.R.R. and D.E.F.. F.C., G.W.C., J.S.W, and R.H. contributed to the design of the work and interpretation of the data. M.G.G. wrote the paper. All coauthors commented critically on the manuscript.

**Competing Interests** The authors declare that they have no competing financial interests.

**Correspondence** Correspondence and requests for materials should be addressed to Martin Gorman(email: gorman11@llnl.gov).